

Differential Emission Measure Distribution Measurement of Collisionally Ionized Plasma: Application to Hot Stars

Patrick S. Wojdowski, Norbert S. Schulz

Center for Space Research, Massachusetts Institute of Technology

`pswoj@space.mit.edu`

ABSTRACT

We describe a technique to derive constraints on the differential emission measure (DEM) distribution, a measure of the temperature distribution, of collisionally ionized hot plasmas from their X-ray emission line spectra. This technique involves fitting spectra using a number of components, each of which is the entire X-ray line emission spectrum for a single ion. It is applicable to high-resolution X-ray spectra of any collisionally ionized plasma and particularly useful for spectra in which the emission lines are broadened and blended such as those of the winds of hot stars. This method does not require that any explicit assumptions about the form of the DEM distribution be made and is easily automated. We apply our technique to the *Chandra* HETGS spectra of nine hot stars.

1. Introduction

In hot stars, X-rays are emitted in the wind by gas heated in shocks. In most cases, these shocks are thought to result from an instability inherent in the mechanism which drives the wind: absorption of stellar UV radiation in line transitions. In some cases, however, other physical processes may play a role in the heating of gas to X-ray emitting temperatures. For example, in very young hot stars, channeling of the wind by magnetic fields may play a strong role in the formation of the shocks that heat gas to X-ray emitting temperatures (e.g., ud-Doula & Owocki 2002). Among the evidence that X-ray emission from some hot stars may be due to a mechanism other than the instability of the radiative driving mechanism, is the fact that the X-ray spectra of some hot stars are characteristic of emission by plasma of higher temperature than others. In order to better understand the nature of the X-ray emission from hot stars and, therefore, to better understand the nature of the winds of hot stars, we develop a method to derive rigorous constraints on the distribution in temperature of X-ray emitting plasma in collisional ionization equilibrium from its X-ray emission line spectrum and apply this method to *Chandra* HETGS spectra of 9 hot stars.

The unprecedented spectral resolution of the grating spectrometers on the *Chandra* and *XMM* observatories allows many emission lines to be resolved in observations of objects that are spatially compact and contain an optically thin, hot ($> 10^6$ K) gas in collisional excitation equilibrium. This class of objects includes the shock-heated gas in the winds of hot stars as well as the coronae of cool stars, and some cataclysmic variable stars (see, e.g., Paerels & Kahn 2003). In collisional ionization equilibrium, X-ray line emissivities depend on temperature and density and may also be affected by ambient radiation, especially in the UV. Compilations of the emissivities of X-ray lines as a function of density and temperature have long been available (e.g., Raymond & Smith 1977; Mewe, Gronenschild, & van den Oord 1985; Smith et al. 2001). Compilations of the dependence of line emissivities on the ambient radiation field are also available (e.g., Porquet et al. 2001). Therefore, given a detailed model of an astrophysical object, it is straightforward to compute the emission line spectrum of any optically thin plasma in collisional ionization equilibrium in the object. By comparing computed spectra to observed spectra models may be falsified.

Explicit models of the X-ray emitting plasma in hot stars do exist. However, the theory of X-ray emission in stellar winds is not sufficiently advanced that firm conclusions can be drawn from simple comparisons of models to data. Therefore, in this paper, we take an inductive approach. For the purpose of determining luminosities of most emission lines, the three dimensional temperature and density distributions may be reduced to the differential emission measure (DEM) distribution, which describes the distribution of the material with temperature and which we define in §3. In this paper, we develop a method for obtaining constraints on the DEM distribution of a collisionally ionized plasma from its X-ray emission line spectrum. Because the temperature of the X-ray emitting plasma depends on the speeds of the shocks that heat it, the DEM distribution indicates the distribution of shock speeds in the wind. The DEM distribution is also of particular interest because it is related to the cooling rate and, therefore, the energetics of the X-ray emitting plasma.

Our method consists of fitting the observed spectral data using a model consisting of a continuum plus a number of line emission components, with each line emission component containing all of the lines of a single ion. Since each ion emits only in a specific temperature range, the best fit magnitude for the line emission of a given ion gives a measure of a weighted average of the DEM distribution in that temperature range times the abundance of that element. We plot the constraints for all of the ions are plotted as a function of the ions' characteristic temperatures. These plots may be understood as one-dimensional “images” of the DEM distributions in that they consist of discrete “pixels” (one for each ion) and differ from the true DEM distribution by a convolution which may be understood as a “temperature-spread” function. By fitting the spectrum globally, rather than measuring line fluxes individually, we take advantage of the information available from blended lines.

This is particularly important in the analysis of the spectra of winds of high-mass stars because, in many cases, the high speeds of the winds result in significant broadening and blending of lines. Furthermore, this method can be automated, facilitating the analysis of large numbers of spectra. This last attribute will become increasingly important with the future *Constellation-X* mission which will be able to obtain high-resolution spectra for a large number of hot stars. While we are unaware of any use of this method exactly as it is described here, it is quite similar to and, in fact, inspired by methods described by Pottasch (1963) for the analysis of solar ultraviolet spectra, by Sako et al. (1999) for the analysis of an X-ray spectrum of the photoionized wind of the high mass X-ray binary Vela X-1, and by Behar, Cottam, & Kahn (2001) for the analysis of the X-ray spectrum of the corona of the cool star Capella.

In §2 we describe our sample of nine early-type stars which have been observed with *Chandra*/HETGS, the data, and our reduction of it. In §3 describe our method in detail, test in on simulated spectra of single-temperature plasmas and apply it to nine hot stars which and the results of applying our method to the data from our sample of high-mass stars. In §4 we discuss the implications of our results.

2. Data Selection & Reduction

We obtained the data from observations of nine bright O stars with *Chandra* with the High-Energy Transmission Grating Spectrometer (HETGS) in the optical path. In Table 1, we list these nine stars, the distances and interstellar absorption columns to them that we adopt, and the effective exposure times, *Chandra* Observation ID numbers and any references for the *Chandra*/HETGS observations of them.

For all of the stars in our sample, our analysis proceeds from binned count spectra (PHA files), instrument effective areas and exposure times (ARF files), and wavelength redistribution functions (RMF files). For θ^1 Ori C we use the spectral data and instrument response files described by Schulz et al. (2003). For all of the other stars, we use the following procedure. We use spectra extracted as part of the standard pipeline processing done by the *Chandra* X-ray Center. We calculate the appropriate effective area and exposure time for the positive and negative first orders of the the High Energy Grating (HEG) and the Medium Energy Grating (MEG) for each observation using a standard procedure¹. For each of the two gratings we add the spectra and effective areas for the positive and negative first orders. For those stars observed in two pointings, we add the spectra and exposure

¹see <http://asc.harvard.edu/ciao/threads/>

times and average the effective areas for the two pointings. In all cases we use the standard redistribution functions. The background expected for these spectra is very low and we make no correction for it.

3. The Differential Emission Measure Distribution and its Determination

In a collisionally ionized equilibrium plasma, line emissivities depend on temperature, density, and ambient radiation field. In the limit of low density and low radiation intensity, the “nebular approximation”, the approximation that excited ions always decay before they can be excited further, is valid. It has already been demonstrated that the line emission from hot stars cannot be explained by emission from gas in which the nebular approximation is valid. Kahn et al. (2001) have measured ratios of the fluxes of the forbidden lines ($2^3S \rightarrow$ ground) to those of the intercombination lines ($2^3P \rightarrow$ ground) for helium-like ions in the *XMM/RGS* spectrum of ζ Pup and found the values to be lower than expected for the nebular approximation. They point out that the low values they measure are due to excitation of ions in the excited 2^3S state to the 2^3P state by ultraviolet photons from the stellar photosphere. However, for clarity, in §3.1 we first define the DEM distribution and describe a method for deriving constraints on it from an observed emission line spectrum in the context of the nebular approximation. Then, in §3.2, we describe a modified version of this method for deriving constraints on the DEM distribution where the nebular approximation is not valid.

3.1. Nebular Approximation

In the nebular approximation, at given temperature, the volume emissivity of a line is proportional to the square of the density times the abundance of the emitting element. The proportionality to the square of the density is due to the fact that excitation, ionization, and recombination are all due to single ion-electron collisions. Therefore for the purpose of determining line luminosities (and also continuum luminosities), the temperature and density distribution can then be reduced to the the differential emission measure distribution (DEM) distribution:

$$\mathcal{D}(T) \equiv \frac{dE}{d \log T} \quad (1)$$

where T is the electron temperature and E is the emission measure defined as

$$E(T) \equiv \int^T n_e n_{\text{H}} dV \quad (2)$$

Table 1. Stars and Data in our Study

HR #	HD #	Name	Type	Adopted Values			Obs IDs	References ^k			
				Distance (pc)	Absorption (10^{20} cm^{-2})	Exposure (sec)		Type	Distance	Absorb	Data ^a
3165	66811	ζ Pup	O4I(n) ^f	450	1.0	68,598	640	24(22)	10,11	15	1
1895	37022	θ^1 Ori C ^j	O4–6p var	450	19	82,975	3,4	26(22)	15	5	5,6
8281 ^b	206267A	...	O6.5V((f)) ^d	800	30	72,557	1888,1889	25(22)	12	16	...
2782	57061	τ CMa	O9II	1480	5.8 ^c	87,095	2525,2526	24(22)	7	7	...
1899	37043	ι Ori	O9III ^e	440	2.0	49,917	599,2420	25(22)	13	15	...
1852	36486	δ Ori A	O9.5II ^h	501	1.5	49,045	639	24(22)	15	15	4
1948	37742	ζ Ori A	O9.7Ib ^g	501	3.0	59,640	610	24(22)	15	15	2
6165	149438	τ Sco	B0.2V	132	2.7	59,630	638	23	8(3)	15	3
4853	111123	β Cru	B0.5III ⁱ	110	1.7	74,379	2575	18	8(9)	14	...

References. — (1) Cassinelli et al. 2001; (2) Waldron & Cassinelli 2001; (3) Cohen et al. 2003; (4) Miller et al. 2002; (5) Schulz et al. 2000; (6) Schulz et al. 2001, 2003; (7) Moitinho et al. 2001; (8) Perryman et al. 1997; (9) Alcalá et al. 2002; (10) Brandt et al. 1971; (11) Schaefer, Schmutz, & Grenon 1997; (12) Simonson 1968; (13) consistent with Hillenbrand 1997 and references therein; (14) Code et al. 1976; (15) Berghöfer, Schmitt, & Cassinelli 1996; (16) Shull & van Steenberg 1985; (18) Hiltner, Garrison, & Schild 1969; (22) Maíz-Apellániz et al. 2004; (23) Walborn 1971; (24) Walborn 1972; (25) Walborn 1973; (26) Walborn 1981

^aPrevious publications describing these data from *Chandra*.

^bThe designation HR 8281/HD 206267 includes four stars which we resolve. The spectrum is for HD 206267A.

^cderived using $N_{\text{H}} = 5.8 \times 10^{21} E_{B-V} \text{ cm}^{-2}$

^dHD 206267A consists of stars of type O6.5V((f)) and B0V in a 3.7 day orbit and a third component of type O8V (Harvin et al. 2004).

^espectroscopic binary

^fvariable of BY Dra type

^gemission-line star

^heclipsing binary

ⁱvariable star of beta Cep type

^ja determination of type O7V for θ^1 Ori C has also been made by Conti (1972)

^kReferences in parenthesis indicate a secondary reference.

where n_e is the electron density, n_H is the hydrogen atom density and the integration is over that volume where the temperature is less than T . In addition, because diffuse plasmas in collisional ionization equilibrium cool radiatively, the cooling of gas is also determined by the DEM distribution.

The luminosity of an emission line i from an ion of charge state z of element Z is

$$L_{Z,z,i} = A_Z \int \mathcal{D}(T) P_{Z,z,i}(T) d\log T \quad (3)$$

where A_Z is the abundance of element Z relative to solar and $P_{Z,z,i}(T)$ is the line power function which depends only on atomic physics parameters and the solar abundance of the element. Line power functions have been tabulated for a large number of lines and the Astrophysical Plasma Emission Database (APED, Smith et al. 2001) contains power functions for thousands of X-ray emission lines. Therefore, from the measurement of a line luminosity, a constraint on the product of the elemental abundance and the DEM distribution can be inferred.

In the absence of specific theoretical predictions of DEM distributions, it may be useful to determine, at least approximately, the magnitude and form of the DEM distribution. If we divide Equation 3 by $\int P_{Z,z,i}(T) d\log T$, then it may be seen that the measurement of a line luminosity constrains the product of an elemental abundance and a “weighted average” of the DEM distribution. In Figure 1, we show the power functions of the lines of two ions. The line power data we use in this figure and elsewhere in this paper is from a version of APED based on the publicly released version 1.1 but modified to include the dependence of line power functions to include their dependence on density (R. Smith, private communication 2002). It may be seen in the figure that the line power functions are single-peaked and, compared to their peak values, are negligible outside of temperature ranges of about one decade around each peak. Therefore, the weighted average values of the DEM that we obtain from the measurement of line luminosities are, approximately, the average value of the DEM in the vicinity of the peak of that line’s power function. Measuring the luminosities of several lines with power functions that peak at different temperatures gives us approximate average values of the DEM distribution in several temperature ranges.

As we have previously mentioned, the winds of hot stars have large speeds so many lines are significantly broadened and blended. This may result in an inability to uniquely measure line luminosities, resulting in large correlated errors in the implied average DEM values. In order to avoid such degeneracies, we take advantage of the fact that the power functions of most of the lines, and all of the strong lines, of an ion have very nearly the same shape. This similarity of line power functions is demonstrated in Figure 1. If two lines have power functions that have the same shape but differ by a constant factor, then the ratio

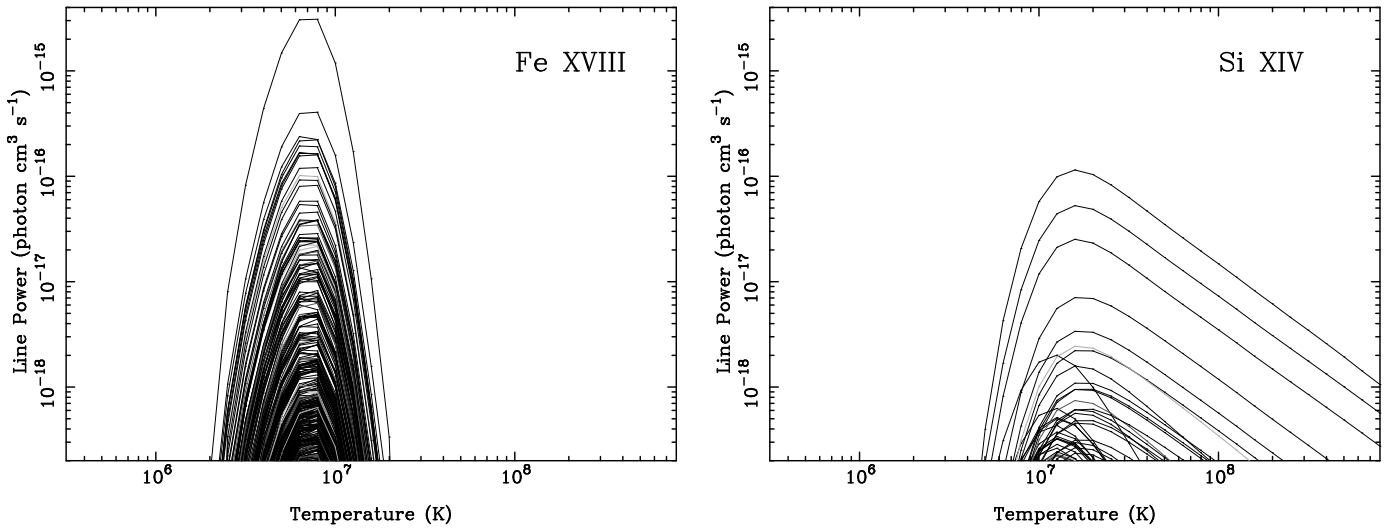


Fig. 1.— Line power functions and summed line power functions for the L -shell ion Fe XVIII and the hydrogen-like ion Si XIV from APED (Smith et al. 2001). The topmost line in each panel is the total line power function (Θ , defined by Equation 4). All lines from the database are plotted. For Fe XVIII, the lines can be seen to have nearly the same temperature dependence. For Si XIV, a family of line power functions have a temperature dependence significantly different from the others, peaking at a lower temperature. However, the peak of this line power function is only a few percent of the peak of the power function of the strongest line. These figures illustrate the validity of our approximation that the line power functions of most of the lines of a given ion, and all of the strongest lines of that ion, the line power functions have almost the same shape.

of the luminosities of those two lines will differ by that same constant factor regardless of the DEM distribution. Therefore, instead of attempting to measure the fluxes of individual emission lines in a spectrum, we fit the entire spectrum, fixing the ratios of the luminosities for the lines of each ion. In such a fit, there is only one free line luminosity normalization parameter for each ion. Just as the luminosities of individual lines imply average values of the DEM distribution in temperature ranges defined by the line power functions, so do these normalization parameters. However, because each ion has a distinct set of lines with distinct luminosity ratios, these normalization parameters and the corresponding average values of the DEM distribution can be uniquely constrained, even if lines are significantly blended. For several ions, there is a family of lines, the dielectronic recombination lines, that have power functions that differ significantly from the other lines of the ion. This fact can be seen in Figure 1 for Si XIV. However, the dielectronic lines are quite weak. The peak powers of the dielectronic recombination lines are only a few percent of those of strongest lines. Therefore, we proceed with our attempt to derive constraints on DEM distributions by fitting spectra with fixed line luminosity ratios.

In order to choose line luminosity ratios for fitting spectra, we define the function $\Theta_{Z,z}$ for each ion as the sum of all of the power functions for all of the lines of that ion:

$$\Theta_{Z,z}(T) \equiv \sum_i P_{Z,z,i}(T). \quad (4)$$

For each function Θ , we define a temperature T_p to be the temperature at which it peaks. We then let the line luminosities be given by

$$L_{Z,z,i} = D_{Z,z} P_{Z,z,i}(T_{p,Z,z}) \Delta_{Z,z} \log T \quad (5)$$

where $D_{Z,z}$ is a variable normalization parameter and

$$\Delta_{Z,z} \log T \equiv \frac{\int \Theta_{Z,z}(T) d \log T}{\Theta_{Z,z}(T_{p,Z,z})}. \quad (6)$$

If all of the line power functions of a given ion have exactly the same shape, then the value of D for that ion gives the weighted average DEM value corresponding to the line luminosities described above. As mentioned above, not all of the line power functions for every ion have the same shape. However, as those line power functions that differ significantly have magnitudes of only approximately 1% of the value of the strongest line power functions, we expect an error due to the difference of line power functions of no more than about 1%.

As we have mentioned before, the X-ray emission line spectra of hot stars differs significantly from what is predicted in the nebular approximation. Indeed, attempts to use the method so far described resulted in very poor fits to the triplets of helium-like ions and,

presumably therefore, inaccurate constraints on the DEM distribution for those ions. Therefore, in order to get good fits to the observed emission-line spectra and accurate constraints on the DEM distribution, it is necessary to alter our method.

3.2. Line Pumping

For most excited states, over the range of physical conditions we will consider, the probability that the further excitation will occur is negligible, as in the nebular approximation. However, atoms in some long-lived (metastable) excited states are susceptible to further excitation by collisions with electrons or absorption of photons. The result of this is that the emission in lines resulting from the decay of the metastable state are “pumped” into emission from lines that result from the decay of the state to which the ion in the metastable state is excited. While photoexcitation is the most relevant pumping mechanism for hot stars, we first consider pumping by collisional excitation only because the effects of the two mechanisms are similar and because data for pumping by collisional excitation is more readily available. For this case, the line emission may still be described by line power functions. However, the line power P is a function of density as well as temperature. Therefore, the emission line spectrum depends on the two-dimensional temperature-density DEM

$$\mathcal{H}(T, n_e) \equiv \frac{d^2 E}{d \log T d \log n_e} \quad (7)$$

The DEM distribution is related to this quantity by

$$\mathcal{D}(T) = \int \mathcal{H}(T, n_e) d \log n_e. \quad (8)$$

If the density dependence of each line power function of a single ion (1) is due to a single upward transition from a single metastable state and (2) the collisional excitation rate for that transition does not change much over the temperature range where that ion emits, then the line power functions for that ion may be well approximated by the form

$$P_{Z,z,i}(T, n_e) = \Theta_{Z,z}(T)(B_{Z,z,i} + F_{Z,z,i}H_{Z,z}(n_e)) \quad (9)$$

where Θ and H are functions that are the same for all of the lines of a given ion and B and F are constant coefficients for each line. Even if the two conditions mentioned above are not satisfied, the line power functions may be well approximated by this form. We discuss the validity of this assumption in §3.2.1 and proceed here with the assumption that the power functions have this form.

We define the functions Θ , and the temperatures where they peak, T_p , as before in the limit of low density where the nebular approximation is valid. With this definition, the functions $H(n_e)$ go to zero as n_e does. If the functions H are continuous, it is possible to show that for any temperature-density DEM distribution $\mathcal{H}(T, n_e)$ with an associated DEM distribution $\mathcal{D}(T) = \int \mathcal{H}(T, n_e) d \log n_e$, there exists, for each ion, a value of the density $n_{Z,z}$ such that the temperature-density DEM distribution $\mathcal{H}'_{Z,z}$ defined as

$$\mathcal{H}'_{Z,z}(T, n_e) \equiv \mathcal{D}(T) \delta(n_e - n'_{Z,z}) \quad (10)$$

produces the same luminosities for all of the emission lines of the ion Z, z as does $\mathcal{H}'_{Z,z}(T, n_e)$. Therefore, we modify the method described above by adopting the variable parameters $n'_{Z,z}$ and let the line luminosities be

$$L_{Z,z,i} = D_{Z,z} P_{Z,z,i}(T_{p,Z,z}, n_{Z,z}) \Delta_{Z,z} \log T \quad (11)$$

where $\Delta_{Z,z} \log T$ is defined as before in Equation 6. Again, $D_{Z,z}$ approximates the product of the elemental abundance and the average of the DEM distribution weighted by $\Theta_{Z,z}(T)$.

3.2.1. Accuracy of the Power Function Approximation

A systematic study of the density dependence of emission lines with wavelengths from 1.2–31 Å has been undertaken by Smith et al. (2002). These authors have made fits to the line powers as functions of density at the constant temperatures 10^6 , $10^{6.5}$, 10^7 , and $10^{7.5}$ K for lines with peak powers exceeding a minimum value and also meeting a criterion for variability with density at each temperature. They found the power functions of most of the lines satisfying those criteria ($\sim 90\%$) could be approximated well using a function of the form

$$P(n_e) = c_0 + c_1 \exp(-n_e/n_1) \quad (12)$$

where c_0 , c_1 , and n_1 are fit parameters. If the density dependence for the line powers of all of the lines of an ion have the form of Equation 12, then Equation 9 is a valid description of the line power functions if, in the temperature range where line emission is significant,

- all of the lines of any one ion have the same value of n_1 and
- for any single line, the ratio of the line power at high density (c_0) to the value at low density ($c_0 + c_1$) and the value of n_1 do not change with temperature.

We have inspected the results of Smith et al. (2002) and found that, for all of the ions we use except Fe XIX, Fe XX, and Fe XXI, most of the lines ($\sim 90\%$) are described by Equation 12

and have values of n_1 that are very close, having a standard deviation of 0.1 or less in $\log n_1$. For those lines, of any ion, that meet the criteria to be fit at more than one temperature, the RMS of the difference between values of $\log n_1$ for the same ion at different temperatures is 0.09 and the RMS of the difference between values of $\log(c_0/(c_0 + c_1))$ (the logarithm of P at high density to the value at low density) is 0.16. In summary, Equation 9 is not exactly satisfied for all ions. However, because most line power functions do not depend on density, it is unlikely that this would cause errors greater than a factor of a few. Because Equation 9 is near to being satisfied for most ions, we expect the actual errors to be much less: not much greater than 10 or 20%.

3.2.2. Radiation

Because metastable states may be photoexcited, line powers are functions not only of temperature and density but also of the mean radiation intensity at the frequencies of the transitions that affect line emission. That is, the line power may be written $P_{Z,z,i}(T, n_e, J_\nu)$ or $P_{Z,z,i}(T, n_e, J_{\nu_{i1}}, J_{\nu_{i2}}, \dots, J_{\nu_{im}})$ where J_ν is the mean radiation intensity as a function of frequency $J_{\nu_{ij}}$ are the mean radiation intensities at the frequencies of the transitions affecting line i . While this is, in principle, a large number of variables, the number of transitions in which photoexcitation plays a significant role (the value of m) is often only one. Furthermore, in the vicinity of a hot star,

$$J_\nu = I_{\star,\nu} W \quad (13)$$

where $I_{\star,\nu}$ is the radiation intensity at the surface of the star and is approximately that of a blackbody with a temperature, depending on the stellar type, of a few tens of thousand K and W is a factor accounting for the geometrical dilution of the stellar radiation with distance from the star. We know of no systematic study (at least, not of the scope of that by Smith et al. 2002 for density) of the dependence of line powers on radiation. However, as radiation and density both affect the line power through excitation of metastable stable states, the effects are similar. Therefore, we use the method described above — taking the line emission from each ion to be that at the temperature of that ion’s peak emission and at a single variable density — and assume that the effects of radiation and density can be replicated approximately by density alone. In §3.5, we again address the validity of this approach.

3.3. Implementation

The data base we use has line powers as functions of density in the range 10^6 – 10^{15} cm $^{-3}$ and of temperature in the range 10^4 – 7.9×10^8 K. In all computations described in this paper, line power functions are taken to be zero outside that temperature range. We first determine $T_{p,Z,z}$ and $\Delta_{Z,z} \log T$ for each ion using $n_e = 10^6$ cm $^{-3}$, the lowest density in the database. We then construct the fit functions and fit them to data using ISIS (Houck & Denicola 2000) which contains an interface to the APED database. We use the ISIS thermal/turbulent line profile function:

$$\phi_{Z,z,i}(\lambda) = \frac{1}{\sigma_{Z,z} \lambda_{Z,z,i} \sqrt{2\pi}} \exp \left(\frac{(\lambda/\lambda_{Z,z,i} - (1 + v_r/c))^2}{2\sigma_{Z,z}^2} \right) \quad (14)$$

with

$$\sigma_{Z,z} = c^{-1} \left(\frac{1}{2} v_t^2 + \frac{kT_{p,Z,z}}{m_Z} \right)^{1/2} \quad (15)$$

where m_Z is the mass of element Z , k is Boltzmann’s constant, and v_r and v_t , the radial and turbulent velocities, are variable fit parameters that are the same for all of the lines in the spectral model.

In our analysis we do not attempt to use measurements of the continuum to constrain the DEM distribution. However, in order to fit spectra and obtain accurate constraints from the emission lines, it is necessary to account for the continuum. The continuum emission from a collisional plasma is due primarily to bremsstrahlung, though radiative recombination continua and two-photon continua also contribute. For the continuum model we use a number of bremsstrahlung components sufficient to fit the continuum and let the temperature and normalization of each be free parameters. In all cases, this provides a sufficient empirical representation of the continuum. The decision as to how many bremsstrahlung components are necessary to obtain a good fit to the continuum is made somewhat subjectively. However, this is the only part of the procedure in which human consideration is required for each spectrum.

We simultaneously fit both the HEG and MEG data to find the best fit values of $D_{Z,z}$ and $n_{Z,z}$ for each of the ions by minimizing the Cash (1979) statistic. This statistic, unlike the χ^2 statistic, is valid in the regime where the number of counts in a channel is small such as is the case for several of our data sets. We search for a minimum of the Cash statistic with ISIS, first by using its implementation of the Levenberg-Marquardt algorithm and then using its implementation of the simplex algorithm. We then search for confidence intervals, again using ISIS, on the parameters v_r , v_t , and on each of the values of $D_{Z,z}$ and $n_{Z,z}$. In searching for confidence intervals, only the Levenberg-Marquardt algorithm is used. In

searching for confidence intervals, a new minimum is frequently found, requiring the process to be restarted. On our workstations (with clock speeds of order 1 GHz), fitting and finding all of these confidence intervals for one of our data sets generally takes a few weeks.

3.4. Tests

We tested our method by applying it to a series of simulated spectra. We simulated a spectrum from a plasma with a DEM distribution constant with temperature over the range 3.2×10^5 – 7.9×10^8 K and zero elsewhere. We also simulated spectra from single-temperature plasmas at the temperatures 3×10^5 , 10^6 , 3×10^6 , 10^7 , 3×10^7 , 10^8 , and 3×10^8 K.

The high-mass star ζ Pup is the best-studied star in the X-ray band. Therefore, for our simulations, we use our adopted values of distance and absorption column for ζ Pup. In order to choose a value of the total emission measure for our simulations, we conducted a number of three-temperature fits to the spectrum of ζ Pup. These fits resulted in total emission measures in the range $(2.4\text{--}5.0) \times 10^{55}$ cm $^{-3}$ depending on whether we tried to fit the nitrogen lines or the oxygen lines (this discrepancy is discussed in more detail in §3.5) and we chose a value of 3.6×10^{55} cm $^{-3}$ for the total emission measure. For the constant DEM distribution, this implies a DEM value of 1.0×10^{55} cm $^{-3}$. For our simulated exposure time, we used the exposure time of our observation of ζ Pup. For all of the simulations, n_e was taken to be 8×10^{13} cm $^{-3}$ to simulate the effects on the spectra of UV excitation of metastable excited states. We chose this particular density value because it is large enough so that, like in the actual stellar spectra, the forbidden lines of the helium-like triplets are completely pumped into the intercombination lines. The emission line profile was taken to be that of Equation 14 with $v_r = 0$ and $v_t = 800$ km s $^{-1}$, approximating the line widths observed by Kahn et al. (2001) for ζ Pup.

We fit the simulated spectra using the method described above. To account for the continua, we used three bremsstrahlung components. The fit spectral models also included the same absorption used for the simulation. In Figure 2 we plot the MEG spectrum and values of D vs. T_p for the simulation with constant \mathcal{D} . In the plot of D vs. T_p , the vertical extent of a diamond indicates the statistical error on the best-fit value of D and the horizontal extent of a diamond indicates the temperature range $T_{-,Z,z}$ – $T_{+,Z,z}$ where

$$\log T_{-,Z,z} \equiv \log T_{p,Z,z} - \Delta_{-,Z,z} \log T \quad (16)$$

$$\log T_{+,Z,z} \equiv \log T_{p,Z,z} + \Delta_{+,Z,z} \log T \quad (17)$$

and

$$\Delta_{-,Z,z} \log T \equiv \frac{\int_0^{T_{p,Z,z}} \Theta_{Z,z}(T) d \log T}{\Theta_{Z,z}(T_{p,Z,z})}, \quad (18)$$

$$\Delta_{+,Z,z} \log T \equiv \frac{\int_{T_{p,Z,z}}^{\infty} \Theta_{Z,z}(T) d \log T}{\Theta_{Z,z}(T_{p,Z,z})}. \quad (19)$$

These temperature ranges are the temperature ranges for which the values of $D_{Z,z}$ represent the approximate average values of the DEM. While we do not assess the quality of the spectral fit quantitatively, it may be seen that the fit is quite good. In Figure 3, we show the plots of $D_{Z,z}$ for the simulated spectra of single-temperature plasmas. The fits for these spectra, which we do not show, are also quite good. In the first panel of Figure 2 and in Figure 3 we use the same temperature range on the horizontal axis and 3 orders of magnitude in DEM on the vertical axis. This allows slopes of lines in the various plots of to be compared. Our best-fit values of v_t and v_r have uncertainties of a few tens of km s^{-1} and are consistent with the input values of 800 km s^{-1} and zero, respectively.

It may be seen from Equation 3 that, for a constant DEM distribution, we expect the values of $D_{Z,z}$ to be that constant value of the DEM and, as illustrated in the first panel of Figure 2, within the errors, this is indeed what we find. This, and the good quality of the fits indicates that the fact that not all of the power functions of every ion have the same temperature dependence does not cause our method to be significantly inaccurate. As our simulated plasma has only a single density, this does not test whether or not deviations in the line power functions from the form of Equation 9 cause significant inaccuracies in our DEM determinations. Using plasmas with distributions of densities would have provided a test of this. However, this would not have provided a test of the accuracy of our method for plasmas with strong ambient radiation fields. Simulating the emission of a plasma with an ambient radiation field is beyond the scope of this work.

For each of the single temperature simulations, the determined values of $D_{Z,z}$ show a peak at the temperature of the simulated plasma. However, the sharpness of the peak differs for each of the simulations. These plots may be understood as “temperature-spread functions” in analogy with point spread functions in images for use in evaluating our results from observed spectra.

3.5. Stars

We applied our procedure to the spectra of each of the stars listed in Table 1. In each our fits to the stellar data, we used two bremsstrahlung components except in the case of

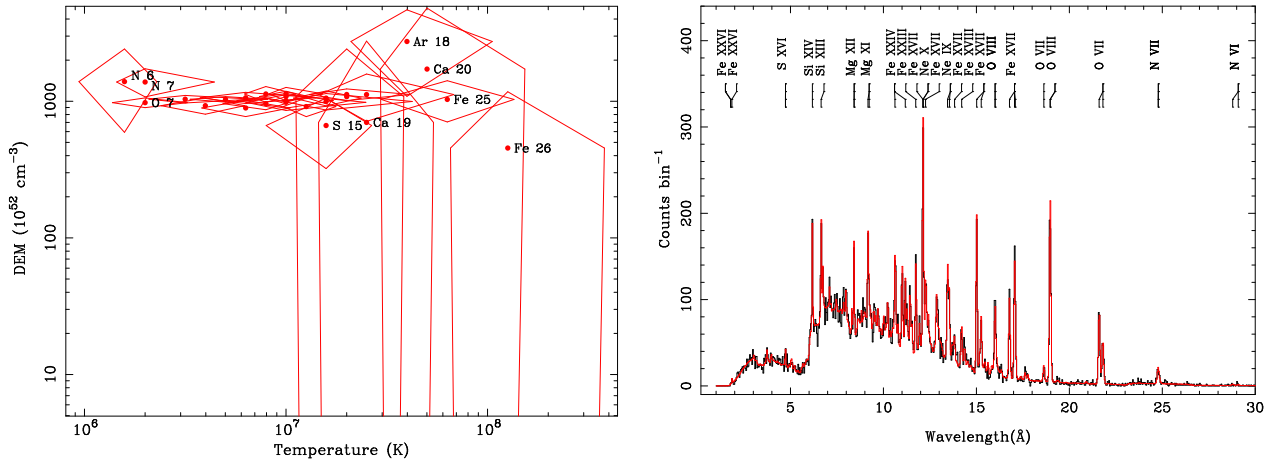


Fig. 2.— In the first panel, the results for the simulated data for a DEM constant in the range 3.2×10^5 – 7.9×10^8 K ($\mathcal{D} = 1.0 \times 10^{55}$ cm $^{-3}$) is plotted. For each ion Z, z , we plot a filled circle at $(T_{p,Z,z}, D_{Z,z})$ where $D_{Z,z}$ is our best-fit value. The vertical extent of the diamond around a filled circle indicates the confidence region determined for $D_{Z,z}$ and the horizontal extent of the diamond indicates the region $T_{-,Z,z}$ – $T_{+,Z,z}$, which is defined in the text and is, approximately, the region over which the ion emits. The ions corresponding to the data points are labeled using Arabic numerals rather than Roman numerals. Because the data points are so close in this plot, we label only a few of them. In the second panel we show the simulated MEG spectrum (black) and the best-fit model obtained with our method (red). We label several bright lines. Though we do not show it here, the HEG spectrum was also used in the fit. For this and all of our simulated spectra, we adopt the absorption column (1.0×10^{20} cm $^{-2}$), total emission measure (3.6×10^{55} cm $^{-3}$) emission measure, line width (800 km s $^{-1}$) of ζ Pup.

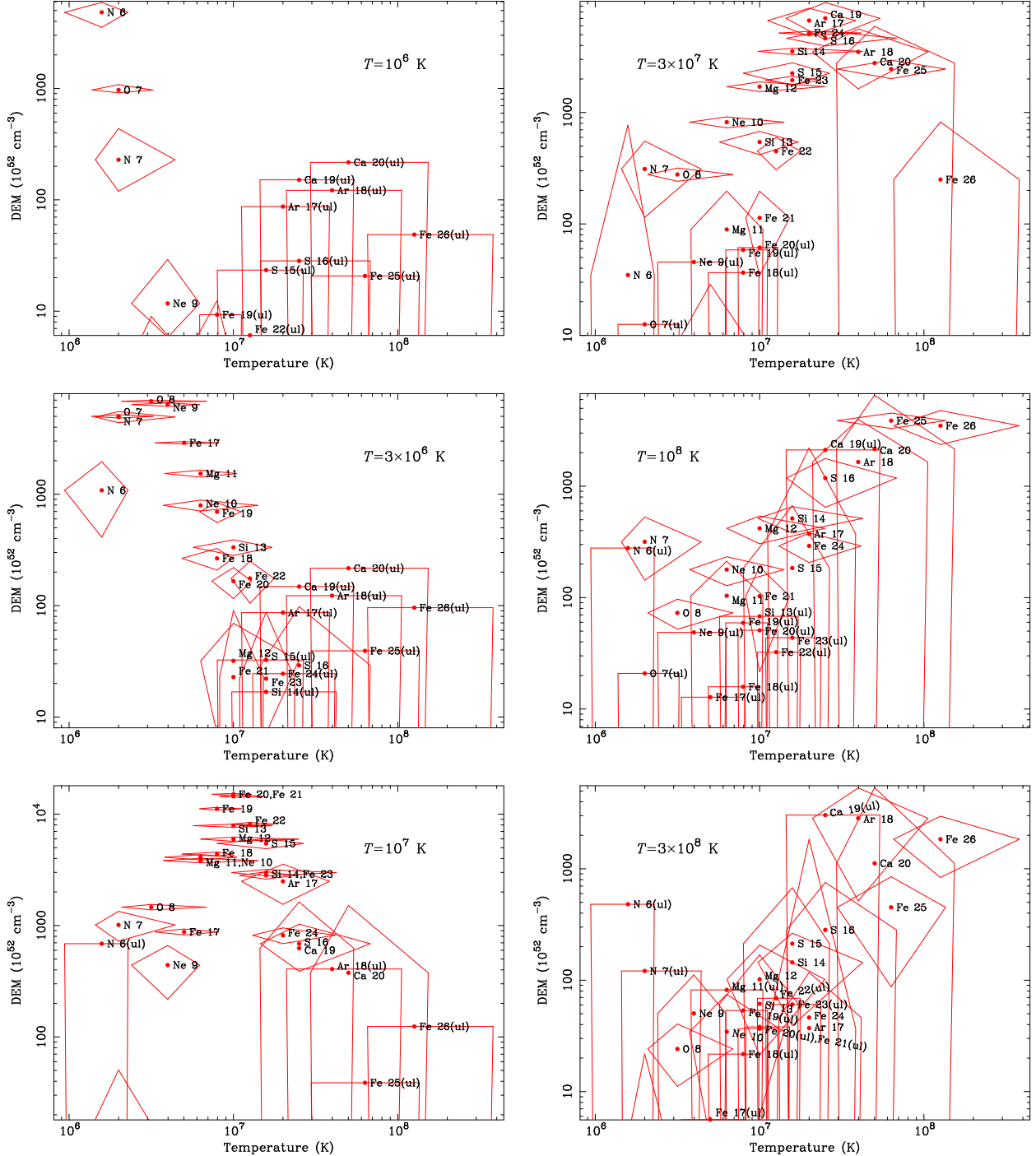


Fig. 3.— Plots of DEM constraints for spectra of plasmas at the single temperatures 10^6 , 3×10^6 , 10^7 , 3×10^7 , 10^8 , and 3×10^8 K. The designation “(ul)” indicates an upper limit.

τ Sco, θ^1 Ori C, and ζ Ori where three were necessary to fit the continuum. In each case, the model spectrum included absorption fixed at the value listed in Table 1. In Figures 4 and 5 we show the constraints on the DEM distributions of the stars that we obtain. In these plots, we use the same temperature range on the horizontal axis as in previous plots and, also as in previous plots, three orders of magnitude on the vertical axis so that slopes of lines may be compared. In Table 2 we show the best-fit values of the parameters v_r and v_t . While we have not quantitatively assessed the quality of the fits, it may be seen from the spectral plots that the fits are quite good considering the large number of lines apparent in the data. The fact that the spectra are well fit indicates that the pumping of lines is well accounted for and that we do not expect significant errors due to line pumping.

In the plots of D vs. T_p , for nearly every two ions with close values of T_p , the corresponding values of D generally appear to be consistent with each other or differ by no more than a factor of two, indicating that the emission line spectrum is consistent with emission from a plasma with solar abundances. One exception to this is the fact that, for ζ Pup, the values of D for oxygen, are approximately an order of magnitude less than the values for ions with similar values of T_p . A similar result has been obtained by Kahn et al. (2001). The values of D for nitrogen appear to fit better with the rest of the data points than do the values for oxygen. Therefore, it is probably the case that oxygen is underabundant in the wind of ζ Pup. However, from this analysis alone, it is impossible to exclude the possibility that the DEM distribution of ζ Pup peaks at approximately 3×10^6 K, that nitrogen is highly overabundant relative to solar and that the abundance of oxygen is nearly solar. In addition, there is significant scatter in the data points for ζ Pup in the temperature range (4×10^6 – 10^7 K). Some, but not all of this scatter would be explained an underabundance of iron. For τ Sco, like ζ Pup, the values of D for oxygen fall below the values for other ions at nearby temperatures, though not by as much. Another exception to our results being consistent with solar abundance is θ^1 Ori C. For this star, most of the values of D appear to lie on a single curve except for those of the ions Fe XX– XXIV which lie below it by a factor of approximately four. Schulz et al. (2003) fit this spectrum using a multi-peaked DEM distribution and a set of metal abundances that differ significantly from solar values. A detailed comparison of the two analyses is beyond the scope of this work. However, our results appear to be consistent with that model.

The line shifts that we measure are generally consistent with zero, with the exception of ζ Pup. The blueshift we find is consistent with the line shifts reported by Kahn et al. (2001) and by Cassinelli et al. (2001). The latter authors attribute this blueshift to obscuration of the far side of wind by photoelectric absorption in nearer parts of the wind.

In order to compare our constraints on the DEM distributions of the stars, we plot a

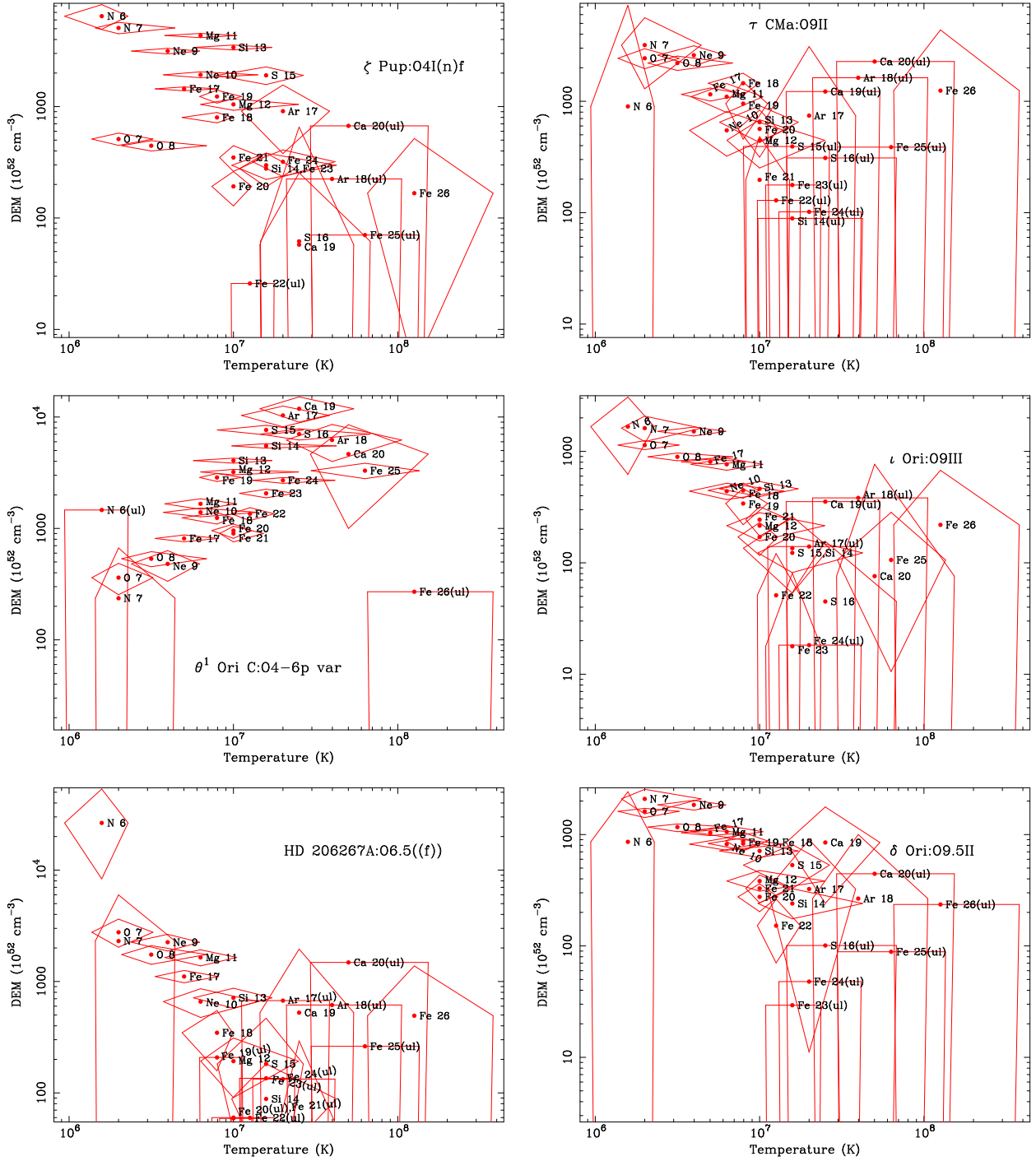


Fig. 4.— DEM constraints for ζ Pup, θ^1 Ori C, HD 206267A, τ CMa, ℓ Ori, and τ Sco.

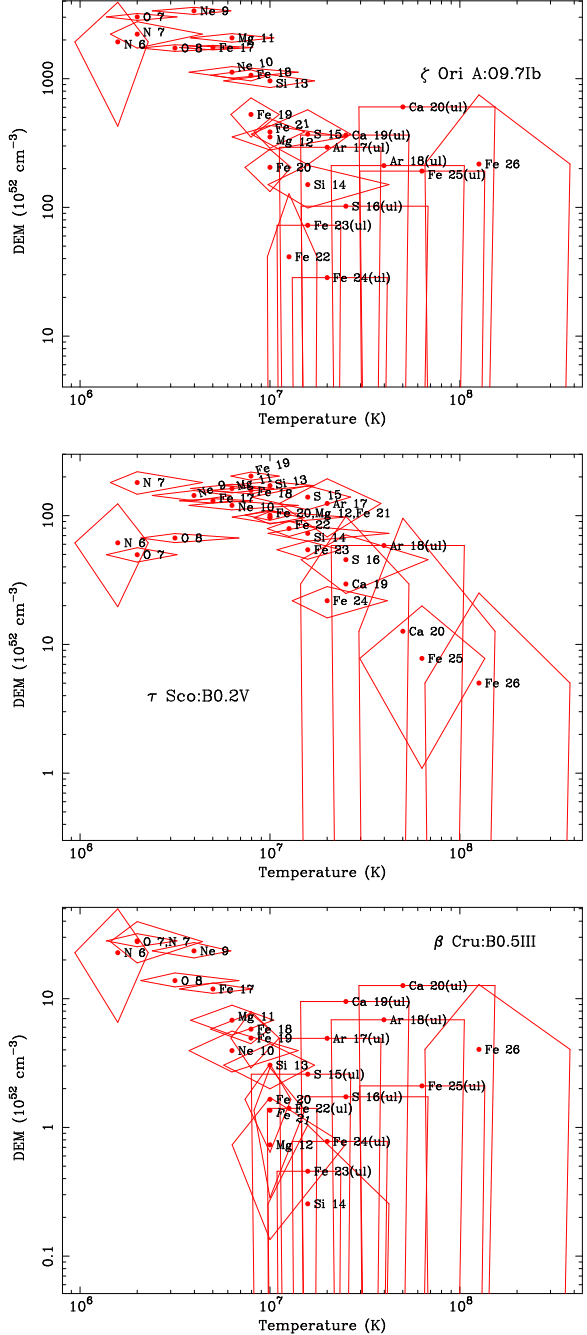


Fig. 5.— DEM constraints for ζ Ori A, δ Ori, and β Cru.

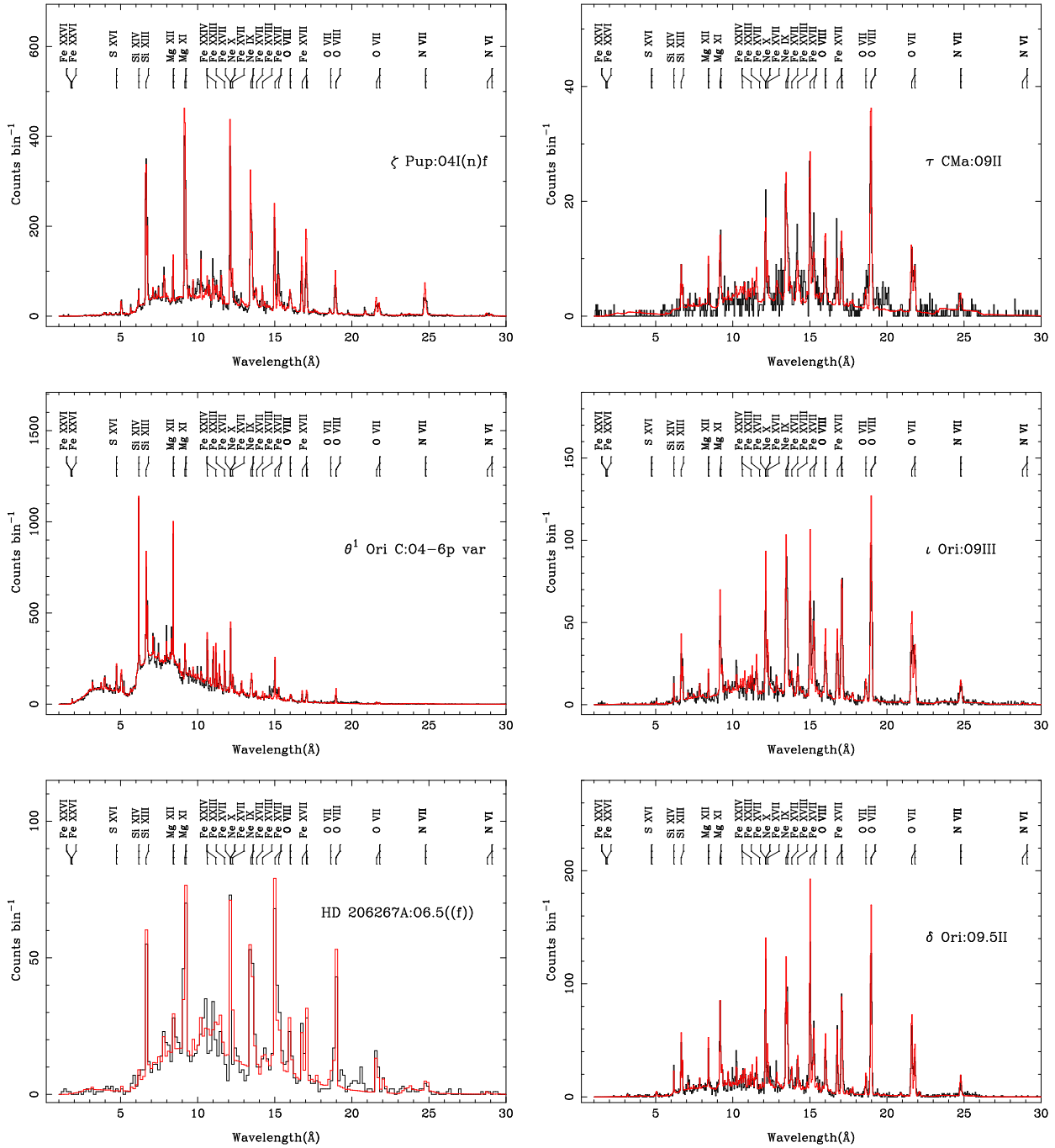


Fig. 6.— MEG spectral data (black) and best-fit models (red) for ζ Pup, θ^1 Ori C, HD 206267A, τ CMa, ι Ori, and τ Sco. We include the line labels from Figure 2 though not all of the labelled lines are present in every spectrum.

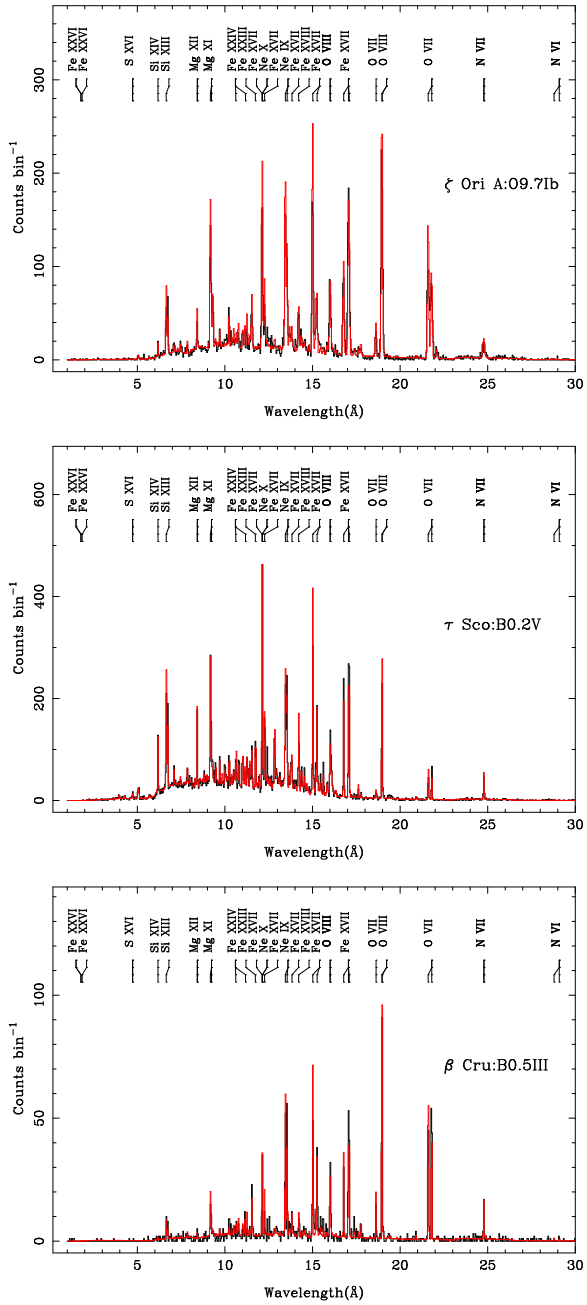


Fig. 7.— MEG spectral data and best-fit models for ζ Ori A, δ Ori, and β Cru.

composite of the nine stars in Figure 8. The construction of this figure is described in the figure caption. With the exceptions of τ Sco and θ^1 Ori C, it may be inferred from these plots that, in the temperature range 10^6 – $10^{8.5}$ K, the DEM distributions are characterized by having peaks and most of their emission measure at temperatures of a few times 10^6 K or less and by declining towards higher temperatures. The DEM distribution of β Cru, in addition to having a smaller magnitude than the other stars, declines more rapidly towards high temperatures. For τ Sco, the peak of the DEM distribution and the majority of the emission appear to be at approximately 10^7 K. Most of the emission measure for θ^1 Ori C appears to lie near 3×10^7 K.

4. Discussion

We have described a method for deriving constraints on the differential emission measure distribution of a collisionally ionized plasma from its X-ray emission spectrum and displaying these constraints in a way that indicates the DEM distribution with the temperature resolution of the line power functions: a few tenths of a decade. In our analysis, we also derive a characteristic line shift and width for each spectrum. Our analysis accounts for line pumping by the ultraviolet radiation from the stellar surface. While we have not explicitly tested the accuracy of our method for the effects of this, the tests we have done, and the fact that our method results in very good fits to the stellar spectra indicates that the systematic inaccuracies in our method are almost certainly smaller than the statistical errors. We intend to post our analysis scripts to the *Chandra* contributed software exchange (<http://asc.harvard.edu/cont-soft/soft-exchange.html>).

We have used this method to determine the DEM distribution for a sample of nine hot stars. For all of these stars except for θ^1 Ori C and τ Sco we find the DEM distributions to be peaked at a temperature of a few times 10^6 K or less or to be declining monotonically through the entire range from 10^6 K to 10^8 K. In contrast, we find that the peak of the DEM distribution of τ Sco is near 10^7 K and the peak of the DEM distribution of θ^1 Ori C is near 3×10^7 K. For those two stars we also find that the emission lines are narrow compared to stars of similar stellar type. High temperatures and narrow lines have previously been found for τ Sco by Cohen et al. (2003) and for θ^1 Ori C by Schulz et al. (2001, 2003) using these same observational data. In both cases, the high temperatures and narrow lines have been attributed to magnetic channeling of the wind. In this scenario, wind travels up the sides of magnetic loops, then shocks as wind from the two sides of the loop collides. Because the post-shock gas is stationary, narrow lines are predicted. The fact that the post-shock gas is stationary also results in a larger velocity difference between the gas before and after the

Star	Type	v_r	v_t
ζ Pup	O5Iaf	-460 \pm 20	770 \pm 20
θ^1 Ori C	O6pe	-29 $^{+15}_{-14}$	326 \pm 18
HD 206267A	O6.5V((f))	-10 \pm 140	1020 $^{+140}_{-130}$
ζ Ori A	O9Iab	-130 \pm 20	689 \pm 19
τ CMa	O9Ib	-120 $^{+100}_{-110}$	990 $^{+100}_{-90}$
ι Ori	O9III	60 \pm 40	930 $^{+40}_{-30}$
δ Ori A	O9.5II	10 \pm 30	690 \pm 30
τ Sco	B0V	37 \pm 10	159 $^{+14}_{-15}$
β Cru	B0.5III	-12 \pm 19	190 \pm 30

Table 2: Fit Line Shifts and Width Parameters

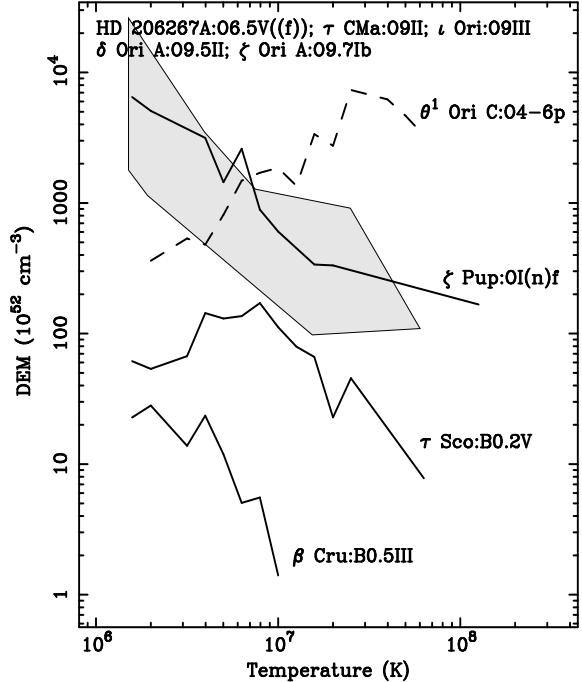


Fig. 8.— A composite of the DEM constraints for the nine stars. For each star, we ignore those values of D without lower limits. For the case of ζ Pup we also ignore the values of D for oxygen. Then, for those ions with the same value of T_p , we average the values of D weighting by the inverse square of the uncertainties. The lines connect the averaged values of D for individual stars. The lines for HD 206267A, ι Ori, ζ Pup, ζ Ori A, τ CMa, and δ Ori A are very similar and difficult to show together. Therefore, we show the line for ζ Pup and a filled polygon that encloses the lines for the other five stars. The axes and aspect ratio of this plot are chosen so that slopes in this figure can be compared with those in Figures 2, 3, 4, and 5.

shock and, therefore, higher temperatures (ud-Doula & Owocki 2002).

The fact that the X-ray emitting plasma in the wind of τ Sco is hotter than the X-ray emitting plasma in most stars has been apparent from spectra of much lower resolution (e.g., Cohen, Cassinelli, & Macfarlane 1997; Cohen, Cassinelli, & Waldron 1997). A hot X-ray emitting plasma has also previously been detected from the Orion Trapezium cluster which contains θ^1 Ori C (Yamauchi et al. 1996) though it was not until a high-resolution image was obtained with *Chandra* by Schulz et al. (2001) that this hot plasma could be conclusively associated with θ^1 Ori C. Therefore, our finding that the temperatures of the X-ray emitting plasmas θ^1 Ori C and τ Sco are high is neither new result of high-resolution spectroscopy or of our analysis technique. However, as we have shown, high-resolution spectra in combination with our analysis technique can provide well-defined quantitative constraints on elemental abundances and differential emission measure distributions. We expect that these results and the results of similar observations and analyses will provide direction for developing theory on the development of theory on X-ray emission in hot stars.

We expect that the technique described here will be useful in the analysis of high-resolution spectra of plasmas in collisional ionization equilibrium in astrophysical contexts other than hot stars. This technique is particularly useful in cases where lines are broadened to the point of being blended. Mukai et al. (2003) have shown that the X-ray spectra of some cataclysmic variable stars are characteristic of plasmas in collisional ionization equilibrium. Some of those spectra show lines as broad as 500 km s^{-1} . Even for spectra in which lines are not broad and blended, this technique has advantages over others. It does not require fitting of individual lines to determine their fluxes and is therefore easily automated. Also with this technique, it is not necessary to make assumptions or introduce biases about the form of the DEM distributions. Therefore, our technique may also be useful for analysis of high-resolution spectra of the coronae of cool stars obtained with *XMM* and *Chandra*. The *Astro-E II* observatory will be able to obtain high-resolution spectra of extended objects. Therefore, with the data from that observatory, our technique may be useful in the analysis of the spectra of clusters of galaxies and halos of elliptical galaxies. The fact that this algorithm can be easily automated may be of particular importance when the DEM distributions need to be determined for a large number of spectra. The fact that the anticipated *Constellation-X* observatory will have a very large effective area for high-resolution spectroscopy enable it to obtain spectra for a large number of objects that are too faint to be efficiently observed with the three previously mentioned observatories. Therefore, our technique may be especially useful in the analysis of the large number of high-resolution X-ray spectra that will be obtained with that observatory.

We thank Dan Dewey for a careful reading of the manuscript. This research has made

use of the SIMBAD database, operated at CDS, Strasbourg, France. This research has also made use of the Chandra Data Archive, part of the Chandra X-Ray Observatory Science Center, which is operated for NASA by the Smithsonian Astrophysical Observatory.

REFERENCES

Alcalá, J. M., Covino, E., Melo, C., & Sterzik, M. F. 2002, A&A, 384, 521

Behar, E., Cottam, J., & Kahn, S. M. 2001, ApJ, 548, 966

Berghöfer, T. W., Schmitt, J. H. M. M., & Cassinelli, J. P. 1996, A&AS, 118, 481

Brandt, J. C., Stecher, T. P., Crawford, D. L., & Maran, S. P. 1971, ApJ, 163, L99

Cash, W. 1979, ApJ, 228, 939

Cassinelli, J. P., Miller, N. A., Waldron, W. L., MacFarlane, J. J., & Cohen, D. H. 2001, ApJ, 554, L55

Code, A. D., Bless, R. C., Davis, J., & Brown, R. H. 1976, ApJ, 203, 417

Cohen, D. H., Cassinelli, J. P., & Macfarlane, J. J. 1997, ApJ, 487, 867

Cohen, D. H., Cassinelli, J. P., & Waldron, W. L. 1997, ApJ, 488, 397

Cohen, D. H., de Messières, G. E., MacFarlane, J. J., Miller, N. A., Cassinelli, J. P., Owocki, S. P., & Liedahl, D. A. 2003, ApJ, 586, 495

Conti, P. S. 1972, ApJ, 174, L79

Harvin et al. 2004, in prep.

Hillenbrand, L. A. 1997, AJ, 113, 1733

Hiltner, W. A., Garrison, R. F., & Schild, R. E. 1969, ApJ, 157, 313

Houck, J. C. & Denicola, L. A. 2000, in ASP Conf. Ser. 216: Astronomical Data Analysis Software and Systems IX, 591

Kahn, S. M., Leutenegger, M. A., Cottam, J., Rauw, G., Vreux, J.-M., den Boggende, A. J. F., Mewe, R., & Güdel, M. 2001, A&A, 365, L312

Maíz-Apellániz, J., Walborn, N. R., Galué, H. Á., & Wei, L. H. 2004, ApJS, 151, 103

Mewe, R., Gronenschild, E. H. B. M., & van den Oord, G. H. J. 1985, A&AS, 62, 197

Miller, N. A., Cassinelli, J. P., Waldron, W. L., MacFarlane, J. J., & Cohen, D. H. 2002, ApJ, 577, 951

Moitinho, A., Alves, J., Huélamo, N., & Lada, C. J. 2001, ApJ, 563, L73

Mukai, K., Kinkhabwala, A., Peterson, J. R., Kahn, S. M., & Paerels, F. 2003, ApJ, 586, L77

Paerels, F. B. S. & Kahn, S. M. 2003, ARA&A, 41, 291

Perryman, M. A. C., et al. 1997, A&A, 323, L49

Porquet, D., Mewe, R., Dubau, J., Raassen, A. J. J., & Kaastra, J. S. 2001, A&A, 376, 1113

Pottasch, S. R. 1963, ApJ, 137, 945

Raymond, J. C. & Smith, B. W. 1977, ApJS, 35, 419

Sako, M., Liedahl, D. A., Kahn, S. M., & Paerels, F. 1999, ApJ, 525, 921

Schaerer, D., Schmutz, W., & Grenon, M. 1997, ApJ, 484, L153

Schulz, N. S., Canizares, C., Huenemoerder, D., Kastner, J. H., Taylor, S. C., & Bergstrom, E. J. 2001, ApJ, 549, 441

Schulz, N. S., Canizares, C., Huenemoerder, D., & Tibbets, K. 2003, ApJ, 595, 365

Schulz, N. S., Canizares, C. R., Huenemoerder, D., & Lee, J. C. 2000, ApJ, 545, L135

Shull, J. M. & van Steenberg, M. E. 1985, ApJ, 294, 599

Simonson, S. C. I. 1968, ApJ, 154, 923

Smith, R., Brickhouse, N., Liedahl, D., & Raymond, J. 2002, at http://asc.harvard.edu/atomdb/features_density.html

Smith, R. K., Brickhouse, N. S., Liedahl, D. A., & Raymond, J. C. 2001, ApJ, 556, L91

ud-Doula, A. & Owocki, S. P. 2002, ApJ, 576, 413

Walborn, N. R. 1971, ApJS, 23, 257

—. 1972, AJ, 77, 312

—. 1973, AJ, 78, 1067

—. 1981, ApJ, 243, L37

Waldron, W. L. & Cassinelli, J. P. 2001, ApJ, 548, L45

Yamauchi, S., Koyama, K., Sakano, M., & Okada, K. 1996, PASJ, 48, 719